Energetics of small Pt clusters on Pt(111): Embedded-atom-method calculations and phenomenology

Mark C. Fallis
Department of Physics, University of California, Davis, California 95616

Murray S. Daw*
Sandia National Laboratories, Livermore, California 94551

C. Y. Fong
Department of Physics, University of California, Davis, California 95616

(Received 14 July 1994)

We have employed the embedded-atom method (EAM) to predict the structures and energetics of clusters containing up to seven Pt atoms adsorbed on the Pt(111) surface. The calculated cluster binding energies depend primarily on the number of (nearest-neighbor) bonds between the adatoms. Clusters with the same number of adatoms divide, according to their binding energies, into subgroups (bond families) of clusters with a common number of bonds. The typical spread of binding energies in these bond families is less than 0.2 eV, while the separation between neighboring families corresponds to a mean bond strength of about 0.7 eV. Thus the most stable clusters assume geometries which maximize the number of bonds. In addition, we propose a scheme for modeling the energetics of metal adatom clusters on close-packed metal surfaces whose physical basis is the coordination dependence of metallic bonds. With a simple three-parameter model, we predict binding energies of over 20 Pt clusters in excellent agreement with the EAM calculations. The scheme provides a convenient way of including many-atom interactions in the energetics of two-dimensional (2D) metallic clusters, and should, therefore, be useful for studying the equilibrium properties of 2D metallic surfaces.

I. INTRODUCTION

Making reliable predictions for the morphology and stability of adatom clusters on metal surfaces is important for understanding the equilibrium properties of these surfaces. To understand the relationship between cluster shape and stability it is desirable to know which cluster geometries have the highest binding energies. With this goal in mind, we have undertaken a study of Pt clusters on the Pt(111) surface. This technologically important surface is a good candidate for a theoretical investigation for two reasons. First, because it is close-packed, cluster induced surface relaxations will be small and should not complicate the physics as they can on more open surfaces.[1,2] Second, the Pt(111) surface reconstructs only above the relatively high temperature of 1350 K (Ref. 3) [compare this to the Au(111) surface which is reconstructed at room temperature[4]]. Despite this apparent simplicity, the Pt(111) surface has been the subject of many recent experimental[5–8] and theoretical[9–12] studies.

II. METHOD: EAM SLAB CALCULATIONS

The embedded-atom method (EAM) (Ref. 13) is a semi-empirical scheme for computing the total energy of a metallic system. It has proven to be a powerful tool for investigating complicated physics on noble-metal surfaces including adatom cluster energetics.[1,2] To simulate the (111) surface of a semi-infinite fcc Pt crystal, we used a unit cell or "slab" with free surfaces normal to the [111] direction and periodic boundaries normal to the $[1\bar{1}0]$ and $[11\bar{2}]$ directions. The slab dimensions along the two periodic directions were $20a_1$ and $10a_2$, where a_1 (2.77 Å) and a_2 (4.80 Å) are the repeat distances along the $[1\bar{1}0]$ and $[11\bar{2}]$ directions, respectively. The slab contained 15 (111) layers with 400 atoms/layer or 6000-Pt atoms in total. This unit cell was large enough that the difference in binding energy between two large (seven adatom) clusters was converged to within ± 1 meV. We checked the convergence for both chain and island-shaped clusters occupying both fcc and hcp sites. Convergence for the largest clusters guaranteed (at least) the same convergence for smaller clusters.

Before performing calculations with adatoms, the bulk terminated Pt slab was relaxed first. This involved minimizing the total EAM energy of the slab via a conjugate gradients procedure.[14] During this and all subsequent relaxation calculations, the area of all the (111) layers of the slab and spacing between the bottom four were held fixed at their ideal bulk values. This is done, as in Ref. 2, to mimic a semi-infinite crystal and to allow meV convergence with a smaller slab. After relaxation, the spacing between the top two (111) layers of the slab decreased by 3.6%. This is about half of the shrinkage calculated for the Pt(001) surface in Ref. 2, showing the comparative smallness of the surface relaxations on the Pt(111) surface. Using this relaxed slab, the binding energy of each n-atom cluster was calculated by minimizing the total energy of the cluster adsorbed on the slab and subtracting from this the adsorption energy of n isolated

single adatoms. That is, we define the binding energy of an n-adatom cluster to be

$$E_{\text{bind}} = (E_{\text{cs}} - E_s) - n(E_{\text{as}} - E_s) , \quad (1)$$

where E_{cs} is the total energy of the cluster adsorbed on the slab, E_{as} is the total energy of a single atom adsorbed on the slab, and E_s is the total energy of the slab alone (all energies for fully relaxed configurations). With this definition, the binding energy of a cluster is the energy required to dissociate it into isolated adatoms. In all our EAM calculations, we used the empirical platinum functions developed by Voter and Chen.[15,16]

III. CLUSTER TYPES

In this study we confine our attention to planar clusters containing up to seven adatoms, occupying only the (111) layer immediately above the substrate. The clusters we studied can be divided into two major groups: homogeneous-site and mixed-site clusters.

A. Homogeneous-site clusters

Every adatom in a homogeneous-site cluster occupies the same type of site on the substrate surface. Since there are two physically distinct sites on an unreconstructed fcc(111) surface where an adatom prefers to sit (the fcc and hcp sites), for each cluster of a given geometry there are (at least) two distinct configurations for the cluster; an fcc configuration where all adatoms occupy fcc sites, and an hcp configuration where all adatoms occupy hcp sites. This is illustrated in Fig. 1 for a linear tetramer which has an fcc (A) and an hcp (B) configuration. In addition, for some clusters containing adatoms arranged in triangles (equilateral, with legs connecting nearest-neighbor adatoms), both the fcc and hcp configurations can be oriented on the substrate in two physically distinct ways, giving a total of four configurations for that cluster geometry. This is illustrated in Fig. 1 for a triangular trimer, which can be oriented on the substrate so that it is centered over an atom in the substrate ["filled orientation with both fcc (D) and hcp (F) examples] or over a hollow (no atom below) in the substrate ["hollow" orientation again with both fcc (C) and hcp (E) examples]. In the filled configuration (D,F), the trimer bonds to seven nearest-neighbor substrate atoms (shaded atoms lying within the borders drawn around clusters), but in the hollow configuration it bonds to only 6. As we will see, this causes the hollow configuration to have a lower binding energy than the filled configuration. Any larger cluster containing more hollow triangles than filled ones or vice versa will also have "hollow" (G) and "filled" (H) configurations like the hexamer in Fig. 1 (only the fcc configurations are shown for the hexamer, there are also hollow and filled hcp versions). In Fig. 1, we have illustrated *all* the physically distinct orientations for homogeneous-site clusters on an fcc(111) surface.

B. Mixed-site clusters

The other group of clusters we studied was mixed-site, i.e., clusters containing some adatoms on fcc sites and some on hcp sites. We found relatively few stable mixed-site clusters (12 versus 122 homogeneous-site) because most initial mixed-site cluster configurations relaxed into homogeneous-site ones. Only enough mixed-site clusters were studied to establish that they had low binding energies and by no means were all the possibilities exhausted.

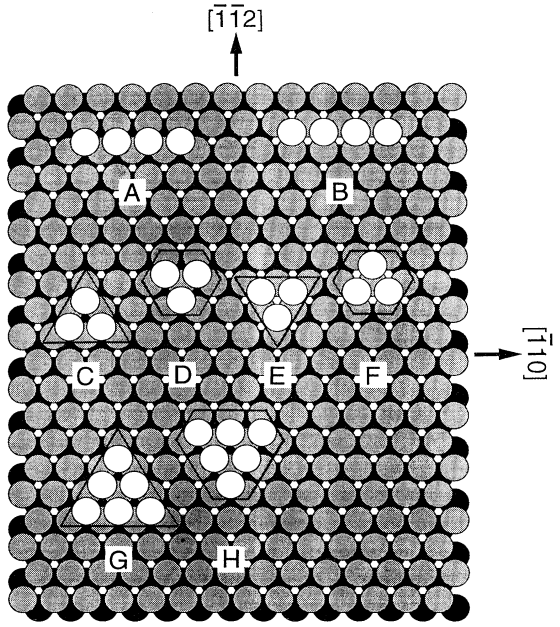

FIG. 1. Several homogeneous-site clusters on the Pt(111) surface as viewed from above along the [111] direction. Pt adatoms (empty circles) are shown lying above the atoms in the first (shaded circles) and second (dark circles) substrate layers (same scheme used in Figs. 2, 3, 6, 8). The four-adatom chain has two configurations, fcc (A) and hcp (B); whereas the trimer and hexamer each have 4: fcc and hcp versions of both "hollow" (C,E,G) and "filled" (D,F,H) configurations (only the fcc examples of the hexamer are pictured).

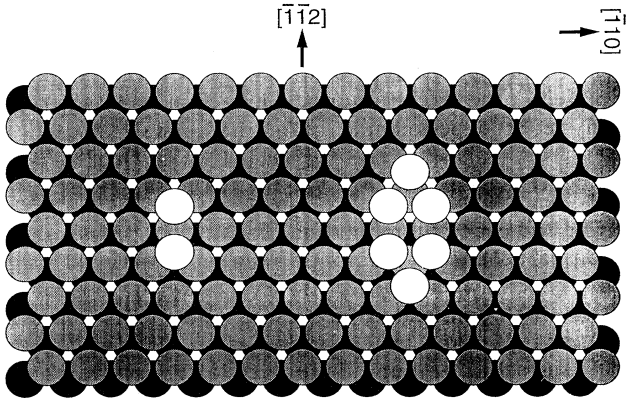

FIG. 2. Two mixed-site clusters on Pt(111) surface; a dimer (left) and hexamer (right).

Two examples of mixed-site clusters are illustrated in Fig. 2; a mixed dimer (left) and a mixed hexamer made of an fcc and hcp triangle joined by two mixed bonds (right). Notice that the mixed bond involves a substrate atom directly between the two bonding adatoms. This stretches and weakens the bond somewhat as compared to the homogeneous-site bond.

IV. RESULTS AND DISCUSSION

A. Cluster binding energies

In this study, calculated cluster binding energies are reported to the nearest meV. This is not to suggest that the EAM is this accurate, but rather to show the small energy differences between some clusters. All the binding energies were calculated according to Eq. (1). The calculated adsorption energies (the difference in total energy between the fully relaxed adatom plus substrate and the relaxed substrate without any adatoms) for a single adatom on an fcc site and on an hcp site are 4.114 and 4.115 eV, respectively.

As a typical example which illustrates some general features common to all the clusters, we show in Fig. 3 the stable fcc configurations of all the (homogeneous-site) four adatom clusters. The binding energies of both the fcc (and hcp) configurations are given below each cluster. The most important point to note from the figure is that the clusters group naturally into families based on the number of nearest-neighbor bonds (black lines) between the adatoms (open circles). All the clusters with the same number of bonds have the same binding energy to within about 0.1 eV. The separation in energy between bond families corresponds to a bond strength of about 0.6–0.7 eV. The cluster with the highest binding energy has the maximum number of bonds.

Two more minor points should be noted. First, the binding energies for the fcc and hcp configurations of each cluster differ by no more than 0.02 eV. In general, for all the clusters, we find the typical difference to be in the meV range with the fcc configuration usually having the higher (more negative) binding energy, especially for the larger clusters. We make no attempt to understand these small (meV) differences since they are out of the EAM's range of accuracy. The second point concerns the four-bond cluster family (two members). As expected, the hollow configuration has a lower binding energy than the filled; by about 0.04 eV in this case. The difference in binding energy between the hollow and filled configurations remains constant for all the (most stable) clusters because they always differ by only one or two more substrate atoms bonded to, independent of the size of the cluster Therefore, as a percentage of the binding energy, this effect should become smaller as the number of adatoms increases, eventually becoming insignificant for very large clusters. In the four adatom case, it amounts to less than 2% of the binding energy and for the hexamer shown in Fig. 1, for which the filled configuration bonds to *two* more substrate atoms than the hollow configuration, it accounts for only 0.5% of the binding energy.

Figure 4 is a plot of the binding energy vs the number of adatoms for all the fcc (homogeneous-site) clusters. The data are spread out horizontally to show more clear-

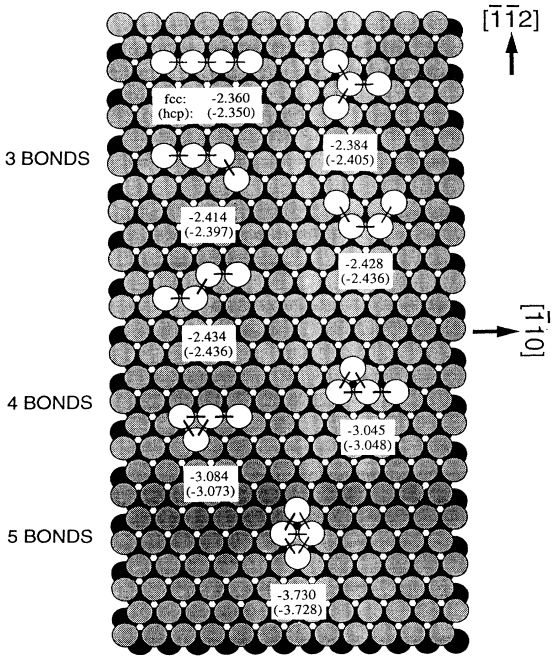

FIG. 3. FCC configurations for *all* the possible (homogeneous-site) four adatom clusters. The binding energies (in eV) for both the fcc and hcp configurations are given below each cluster. The clusters divide into groups (bond families) based on the number of nearest-neighbor bonds (indicated by lines connecting the adatoms) in the cluster. There are five clusters with three bonds, two with four bonds, and one with five.

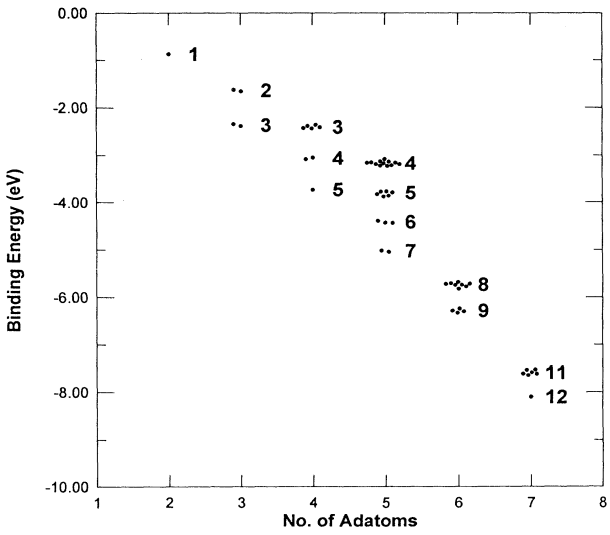

FIG. 4. Binding energies for all the fcc homogeneous-site clusters considered. For each number of adatoms, the clusters divide into bond families with a common number of nearest-neighbor bonds (the number of bonds is given to the right of each family). The data are spread out horizontally to show the population of each bond family.

ly the number of clusters in each bond family (each point represents the binding energy of a distinct cluster). The same trend followed by the four adatom clusters is followed by all the clusters: they group into families whose members all have the same number of bonds. The spread of binding energies for the clusters in these bond families are all less than 0.2 eV, and different families are separated from each other by a bond strength of about 0.7 eV. The most stable or ground-state clusters all have the maximum number of bonds for the given number of adatoms. Notice also that the maximum number of bonds jumps by 2 when going from 2–3–4–5–6 adatoms but then by 3 when going from 6–7 adatoms. The reason for this will be made clear in the next paragraph. Figure 5 is the same plot as in Fig. 4 but for hcp clusters instead and is essentially identical to Fig. 4 in accord with the small (meV) difference between the fcc and hcp cluster binding energies.

Figure 6 shows all of the ground state clusters in their fcc configurations with binding energies labeled as in Fig. 3. All of these clusters have geometries which maximize the number of bonds. When the ground state is "degenerate," with several different clusters that maximize the number of bonds, the one with the highest binding energy will either bond to the most substrate atoms, as for three and five adatoms, or will maximize the number of bonds in the least coordinated fashion, as for the group of four clusters with six adatoms (however, contributions from substrate relaxations may be anomalously high for the six adatom cluster on the far right because of its linear shape). Figure 6 also shows us why the number of bonds jumps by 3 when going from the six adatom to the seven adatom ground state; in making the ground-state heptamer, we can make three bonds instead of the usual two (consider adding an additional adatom to the second hexamer from the right). The above predictions for the most stable clusters agree with similar EAM calculations for Ni clusters on Ni(111).[17] Also, with a few exceptions, the same cluster geometries were observed in studies of Ir clusters on Ir(111) using field-ion microscopy.[18]

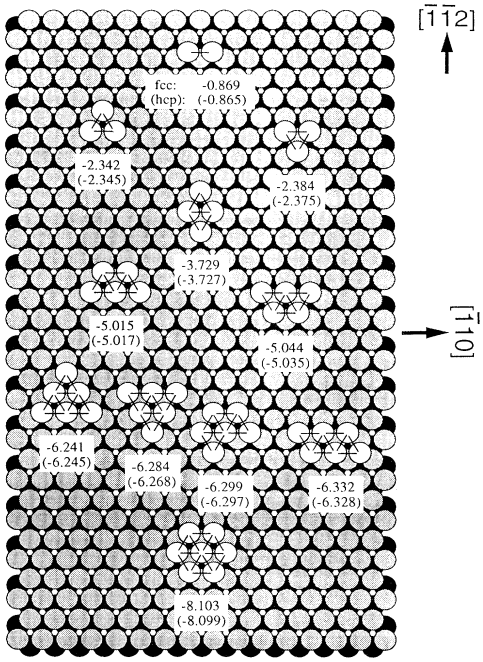

FIG. 6. Predicted fcc ground-state (most stable) cluster configurations and binding energies for both fcc and hcp configurations of Pt clusters with up to seven adatoms. Interadatom bonds are indicated as in Fig. 3..

We now consider mixed-site clusters. In Fig. 7, we have added to Fig. 4 the binding energies of 12 stable mixed-site clusters (empty circles). Clearly, the mixed-site clusters' binding energies all lie at the top or above the first excited sate for the homogeneous-site clusters. To understand why this is so, consider Fig. 8. To form a mixed-site cluster with large binding energy, one would have to start with a highly bound (and therefore, to max-

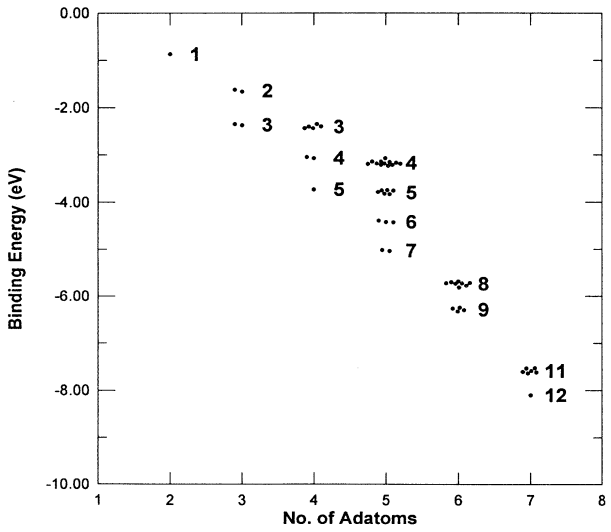

FIG. 5. Binding energies for the hcp configurations of all the clusters in Fig. 4. All details same as Fig. 4.

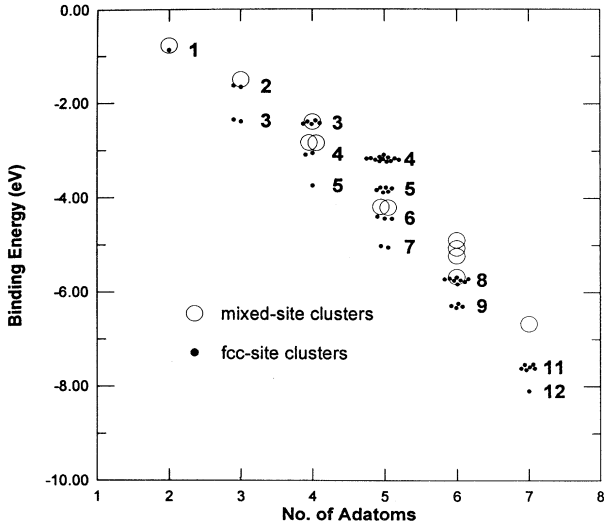

FIG. 7. Binding energies of 12 stable mixed-site clusters added to Fig. 4.

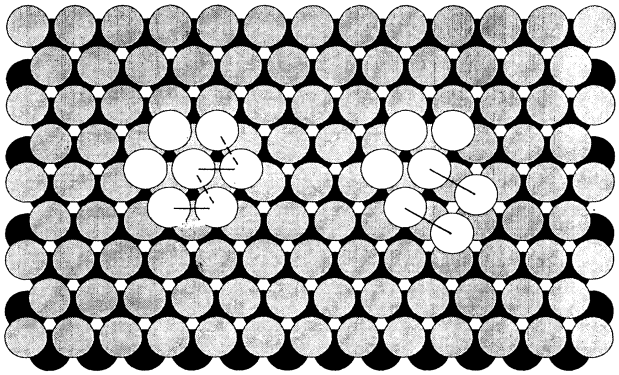

FIG. 8. Diagram illustrating why mixed-site clusters have low binding energies. The energy cost of converting the highly bound hexamer into a mixed-site cluster is about 0.7 eV per shifted adatom for breaking the dashed line bond, and another 0.1 eV for stretching the solid line bond.

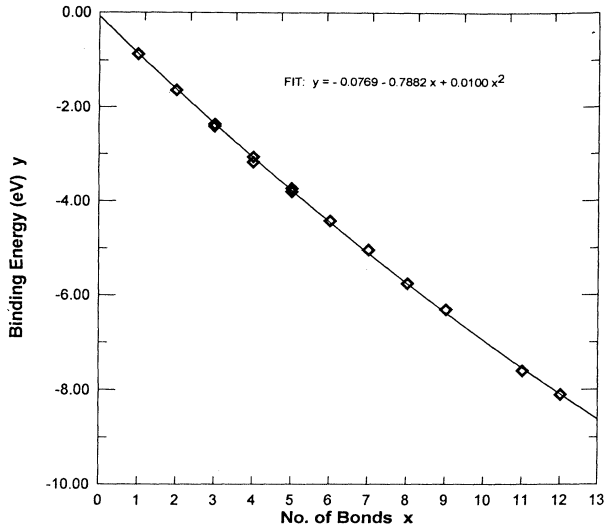

FIG. 9. Mean binding energies averaged over all the fcc- and hcp-site clusters (no mixed-site clusters) in each bond family (see Figs. 4 and 5) plotted against number of nearest-neighbor bonds. The smooth curve is a second degree polynomial (least-squares) fit to the data.

imize the number of bonds, highly coordinated) homogeneous-site cluster and try to shift some of the adatoms to different sites without breaking too many bonds. But it is clear from Fig. 8 that this is impossible to do without breaking one bond (dashed line) per shifted atom. The energy cost of breaking this bond is about 0.7 eV, which will move the mixed-site cluster from the ground state to the first excited state. In addition to breaking a bond, another bond (solid line) must be stretched to make it a mixed bond at a cost of about 0.1 eV [estimated from the binding-energy difference between an fcc dimer (-0.867 eV) and a mixed dimer (-0.773 eV)], which will put the mixed-site cluster at the top of the first excited sate. This is the smallest possible cost for converting a homogeneous-sites cluster to a mixed-site cluster, and as we see from Fig. 7, most of the mixed-site clusters' energies lie well above even the first excited state.

B. Bond counting description of cluster energetics

In Fig. 9, we plot the mean binding energy for each bond family [averaged over all fcc and hcp clusters in the family (no mixed-site clusters)] against the number of nearest-neighbor bonds rather than the number of adatoms. We see that the mean cluster binding energy depends smoothly and monotonically on the number of bonds. This analysis shows that the cluster energetics can be understood in a unified and simple way in terms of the number of bonds between the adatoms: the more bonds a cluster has, the further down on the curve its binding energy lies. It is then natural that the ground-state clusters have the maximum number of bonds. We speculate this type of simple cluster energetics is specific to close-packed surfaces where substrate relaxations do not contribute as much to the cluster binding energies as on more open surfaces such as Pt(001). On this surface, similar EAM calculations reveal, in agreement with FIM measurements, that the ground-state Pt clusters do not always maximize the number of bonds.[19] It is interesting to note that the positive curvature of Fig. 9 is expected from the weakening of the metallic bond with increasing coordination.[20]

Although Fig. 9 allows us to understand the cluster energetics in a simple manner, a lot of detail is lost when we calculate the mean binding energy for each bond family. For example, the binding energies of the four ground-state clusters with six adatoms in Fig. 6 all map to the single point for nine bonds in Fig. 9. In the next section of the paper, we show that a more detailed description of the cluster energetics can be obtained by expressing the cluster binding energies in terms of coordination dependent bonds.

V. ANALYSIS: PHENOMENOLOGICAL MODEL FOR CLUSTERS ENERGETICS

A. Motivation

Ideally, first-principles calculations could be used to make predictions for the geometry and stability of adatom clusters on metallic surfaces which are free of empirical parameters. However, since first-principles simulations of metal surface physics are usually impractical due to lack of symmetry, the traditional approach has been to model the total energy of metallic solids via simple interatomic pair potentials. Unfortunately, pair potentials neglect the coordination dependence of the metallic bond. This many-atom effect is responsible for much of the unique physics which occurs at metallic surfaces.[21] More realistic schemes for modeling metal energetics include the EAM and the related Finnis-Sinclair method,[22] and effective-medium theory.[23] The predictive power of these semiempirical schemes stems from their treatment of important many-atom interactions in a computational-

ly convenient manner.

The EAM (and similar methods) afford detailed study of metal surfaces based on realistic interactions between all atoms of the system (adsorbate and substrate). If the energetics of clusters is determined mainly by adsorbate-adsorbate interactions and less so by interactions involving the substrate, simplified models, such as lattice-gas models, offer a more convenient and transparent simulation method. Even so, it is desirable to include as much physics (as motivated by the EAM or more accurate methods) in the simplified models as possible. For example, many-atom interactions should be included for realistic simulations of metal clusters physics. Workers in the field of two-dimensional (2D) lattice-gas simulations of surfaces typically treat many-atom interactions by adding three-body or "trio" interactions in addition to the pair interaction of the simple lattice-gas Hamiltonian.[24] The trio interaction strengths are either estimated from theory[25] or adjusted to reproduce some specific experimental result.[26] It is assumed that the fully coordination-dependent energetics an be approximated more closely by including some of the important higher n-body terms of its cluster expansion. The shortcoming of this approach is that there are many such terms which must be considered individually.

We propose a scheme for calculating metal adatom cluster energetics as accurately as the full EAM machinery, but which is also simple enough for use in lattice-gas-type simulations of surface energetics. We approach the problem of modifying the simple lattice gas Hamiltonian to include realistic many-atom interactions from a completely different point of view. Instead of using a cluster expansion, we propose a scheme (referred to as the bond saturation model or BSM) for understanding the cluster energetics solely in terms of *coordination-dependent* nearest-neighbor pair interactions. As will be shown, the BSM is equivalent to a lattice-gas Hamiltonian which includes, in addition to the usual two-body interaction, a large number of three and four body interactions as well. Thus, we feel our approach is a much more comprehensive and satisfying scheme for treating many-atom interactions in adsorbate bonding energetics.

B. The bond saturation model (BSM)

From all the clusters whose binding energies are shown in Figs. 4 and 5, we take all of those in the lowest two bond families for each number of adatoms and assign to each distinct cluster *geometry* a mean EAM binding energy averaged over the fcc, hcp, hollow, and filled configurations. Since these are the most stable clusters, they are more likely to be found on a surface after reaching equilibrium. The resulting 22 cluster geometries and their mean EAM binding energies are shown in columns 1 and 4 of Table I, respectively. The maximum deviation from the mean binding energy for the different configurations of each cluster geometry are also shown in parentheses in column 4. Cluster geometries with hollow and filled configurations have the larger deviations (greater than 6 meV). Our aim is to reproduce the mean binding energies with the BSM.

We start with the observation that on an fcc(111) surface like Pt(111), the number of nearest adatom neighbors (coordination) of an adatom in a cluster can vary from 1–6. It is then natural to parametrize the cluster binding energies in terms of six bond parameters, which we label (a)–(f). The parameter a represents the strength of a dimer bond; b, the bond between two threefold coordinated adatoms, etc. For the strength of the bond between two adatoms with different coordination, say z_1 and z_2, we use the arithmetic mean, $[p(z_1)+p(z_2)]/2$, where $p(1)=a$, $p(2)=b$, $p(3)=c$, etc. Thus with only six parameters, we can actually account for many possible bond strengths. In Fig. 10, we illustrate this parametrization scheme for the six cluster geometries, which we used to obtain values for the bond parameters (a)–(f). The chosen clusters increase in complexity from a dimer to a complete monolayer.

By setting the parametrized expressions for the binding energies of these six different clusters equal to the corresponding EAM values, we obtain the following values for the six bond parameters: $a=-0.867$, $b=-0.787\,333$, $c=-0.717\,778$, $d=-0.641\,333$, $e=-0.597\,333$, and $f=-0.551\,667$ (all units eV). These parameters are also plotted in Fig. 11. It should be emphasized that the bond parameters, (a)–(f), exhibit bond weakening with increasing coordination, once again demonstrating that the EAM includes this important many-atom effect. The values of (a) and (f) are determined directly by the mean dimer binding energy and the mean binding energy/adatom of a monolayer, respectively. This way, our scheme is guaranteed to reproduce the EAM binding energies for clusters at opposite ends of the coordination EAM binding energies for clusters at opposite ends of the coordination spectrum. We now show that the number of phenomenological constants in the model can be reduced from 6 to 3.

Figure 11 shows the previously determined bond parameters plotted against nearest-neighbor adatom coordination, z. It is seen that they all lie close to a quadratic function (solid curve) of the form

$$A+Bz+Cz^2 . \tag{2}$$

A least-square fit to the six bond parameters resulted in values for the three coefficients of $A=-0.961\,423$, $B=+0.097\,545\,6$, and $C=-0.004\,861\,16$ (all units eV). This suggests that instead of using six parameters to model the cluster energetics, we adopt a three parameter scheme (the BSM) in which the coordination dependence of the adatom bonds is governed by Eq. (1) and the three coefficients, A–C, are interpreted as phenomenological constants to be determined by fitting to available experimental or theoretical data. Physically, the first two parameters, A and B, determine a straight line which gives the dimer bond strength at low coordination and the weaker (saturated) monolayer bond strength at the maximum coordination of 6. The third parameter, C, provides for the fact that the coordination dependence of bond weakening is not linear but bends over as the coordination is increased.[27] We stress that while the BSM is motivated by fitting to EAM data, in general any avail-

able experimental or theoretical data could be used to determine A, B, and C. In this scheme, the strength of the bond between two adatoms with coordinations, z_1 and z_2, is now given by $A+B(z_1+z_2)/2+C(z_1^2+z_2^2)/2$.

In Table I, we show how well the BSM (three parameter model) reproduces the EAM results. The binding energies predicted by the BSM for the 22 cluster geometries are shown in column 5, with the associated errors in column 6. The BSM and EAM (column 4) binding energies differ by less than 1% for all of the cluster geometries, except the three atom linear chain. We attribute the larger error for the linear chain to a greater percentage of its binding energy coming from substrate relaxations: the EAM binding energies of the three atom chain calculated on a fully relaxed Pt substrate and on a frozen substrate were found to differ by 10.5%, whereas this difference for the other clusters was typically less than 6%. This is presumably due to its special shape, which has a high edge to area ratio and high symmetry.

We have now demonstrated that by fitting to a few (6) clusters to obtain three parameters, one can predict binding energies for all the important cluster geometries essentially as well as the full machinery of the EAM. Again we stress that while we have fit the parameters in the model to EAM data for the Pt(111) surface, the general form can be argued from simple physical motivation (bond saturation) and should apply to any metal where coordination-dependent bonding is dominant.

The BSM rests on the assumption that all adatoms with the same coordination see roughly the same local

Table I. Comparison of EAM and BSM predictions for 22 cluster geometries.

Cluster Geometry	Number of Adatoms	Number of Bonds	Mean EAM Binding Energy (eV)[a]	BSM Binding Energy (eV)	% Error
	2	1	-0.867(2)	-0.869	0.20
	3	2	-1.619(4)	-1.654	2.19
	3	2	-1.655(1)	-1.654	0.03
	3	3	-2.362(21)	-2.357	0.20
	4	4	-3.063(20)	-3.075	0.38
	4	5	-3.728(1)	-3.709	0.51
	5	6	-4.393(2)	-4.373	0.46
	5	6	-4.427(6)	-4.427	0.01
	5	6	-4.432(4)	-4.441	0.21
	5	7	-5.028(15)	-5.007	0.41
	6	8	-5.690(14)	-5.671	0.34
	6	8	-5.723(12)	-5.725	0.03
	6	8	-5.729(14)	-5.725	0.08
	6	8	-5.796(26)	-5.793	0.05
	6	9	-6.260(22)	-6.251	0.14
	6	9	-6.298(1)	-6.266	0.51
	6	9	-6.330(2)	-6.305	0.39
	7	11	-7.531(6)	-7.510	0.28
	7	11	-7.600(16)	-7.564	0.47
	7	11	-7.629(14)	-7.603	0.34
	7	12	-8.101(2)	-8.066	0.43
monolayer	∞	3/adatom	-1.655(2)/adtm	-1.653	0.09

[a] Averaged over all [fcc and hcp (also hollow and filled if applicable)] configurations for each cluster geometry. Numbers in parentheses indicate maximum deviation from mean in meV.

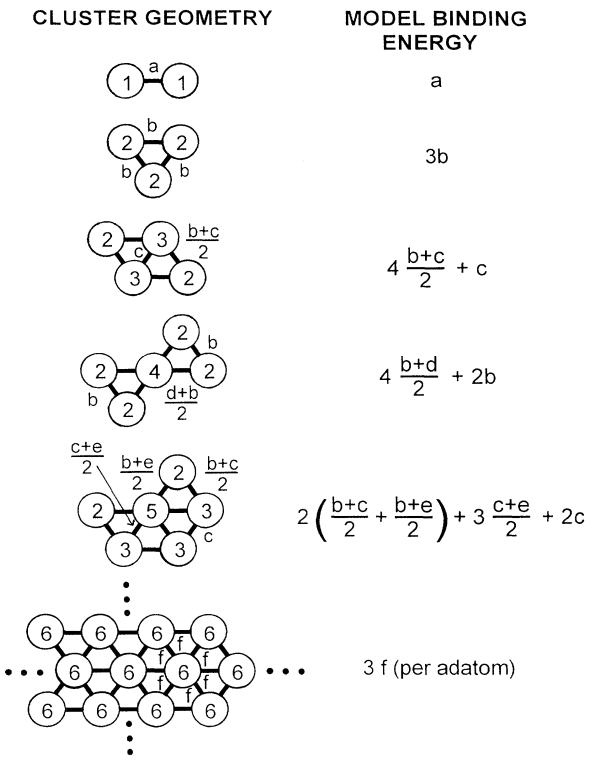

FIG. 10. The six cluster geometries used to obtain the bond parameters (a)–(f) and their corresponding model binding energies. The clusters increase in complexity from a dimer (top) to a complete monolayer (bottom). Cluster adatoms (numbered circles) are labeled by their nearest adatom neighbor coordination, and the interadatom bonds (thick lines) are labeled by their strengths in terms of (a)–(f). The model binding energies are obtained by summing over all the bonds in a given cluster.

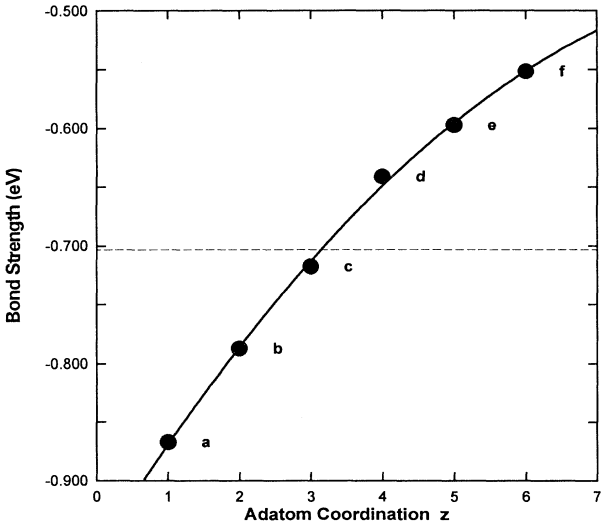

FIG. 11. The six bond parameters (a)–(f), plotted against nearest adatom neighbor coordination. The solid curve is a second degree polynomial, least-squares fit to all six parameters. The dotted horizontal line at -0.7036 eV shows the coordination dependence (or lack of) for the single pair interaction which best fit all the EAM data in Table I.

environment, and, therefore, is best suited to surfaces without large relaxations, such as close-packed surfaces. Also, as with any empirical model, how well it works depends to some degree on the choice of data used to fit parameters. We chose cluster geometries which were widely separated in coordination. By deliberately choosing cluster geometries with low coordination, the maximum error increased to about 3% of the EAM binding energy.

The success of this model is perhaps best appreciated when its predictions are contrasted with a model of cluster energetics via a single pair potential. For example, Table I shows that the BSM is not only able to accurately predict binding energies of clusters with different numbers of bonds, but also to reproduce the correct trends within groups of clusters with the same number of bonds (bond families). If the cluster energetics are modeled by a pair potential, so that every nearest-neighbor bond between the adatoms has the same value independent of coordination, this kind of accuracy and detail is completely lost: all clusters with the same number of bonds would have the same binding energy. By expressing the 22 cluster binding energies in Table I in terms of a single bond strength, s, a least-squares fit to the EAM data resulted in the value of $s=-0.704$ eV. The resulting coordination dependence of the bonding is shown as the dotted horizontal line in Fig. 11. This pair potential scheme under predicts the EAM dimer bond strength by 19% and over predicts the monolayer bond strength by 27.5%. These inaccuracies could adversely affect the predictions of simulations using only pair potentials.

C. BSM as a lattice gas

We now show how the traditional lattice-gas Hamiltonian is modified when the BSM is used in place of a pair potential to characterize the interaction between neighboring atoms on a lattice. The simplest lattice gas Hamiltonian is

$$H=\sum_{i,(j)}\tfrac{1}{2}U_0 n_i n_j \ , \tag{3}$$

where U_0 is a constant pair interaction, and n_i, the particle concentration at site i (0 or 1 only). The summation is taken over all sites i and their nearest-neighboring sites, j (the parentheses are to emphasize that j depends on i). In terms of $z_i=\sum_{(j)}n_j$, the nearest-neighbor coordination at site i, we can rewrite (3) as

$$H=\sum_{i}\tfrac{1}{2}U_0 n_i z_i \ . \tag{4}$$

Replacing U_0 by the BSM nearest-neighbor interaction (2), the above Hamiltonian becomes

$$H_{\rm BSM}=\sum_{i}\tfrac{1}{2}[\,An_i z_i+Bn_i z_i^2+Cn_i z_i^3\,] \ . \tag{5}$$

Using the definition of z_i everywhere in (5) and rearranging the resulting three and four body summations so that none of the site indices in any given term are the same (and using the fact that $n_i=0$ or 1 only), we obtain

$$H_{\mathrm{BSM}}=\frac{1}{2}\left[\sum_{i,(j)}(A+B+C)n_i n_j + \sum_{i,(j,k)}{}'(B+3C)n_i n_j n_k + \sum_{i,(j,k,l)}{}'Cn_i n_j n_k n_l\right]. \quad (6)$$

Here, the primes indicate that none of the nearest-neighbor sites of site i [in parentheses, as in (3)] are repeated. In addition to a pair interaction term [$A+B+C=-0.868\,739$ eV=the dimer bond strength (see Table I)], the BSM includes a large subset of all possible three and four body terms as well. Note that, for fixed i in (6), the number of terms involving i and $n-1$ specific neighboring sites is $(n-1)!$. Taking the sum of these terms as an n-body interaction gives a trio interaction strength of $B+3C$ ($+0.082\,962\,1$ eV), and a quartet interaction strength of $3C$ ($-0.014\,583\,5$ eV). Each trio and quartet has the same interaction strength independent of its shape. While including these many-atom interactions, H_{BSM} in (5) is just as computationally convenient as the two-body Hamiltonian (4), requiring only the values of n_i and z_i at each lattice site.

VI. SUMMARY AND CONCLUSION

To summarize, we have calculated the binding energies for clusters containing up to seven Pt atoms adsorbed on the (111) surface of Pt. Clusters with the same number of adatoms divide into groups (bond families), wherein each cluster has the same total number of nearest-neighbor bonds between the adatoms. The clusters in each bond family have similar binding energies (all within 0.2 eV of each other). The separation in energy between neighboring families corresponds to a bond strength of about 0.7 eV. We find that the most stable clusters assume geometries which maximize the number of bonds between adatoms. We have also shown that the overall cluster energetics can be understood most simply in terms of the number of these bonds.

In addition, we have developed a simple scheme (the bond saturation model or BSM) for modeling the energetics of metallic clusters, which includes the coordination dependence required to realistically treat metallic bonding. Our model involves three phenomenological parameters which we obtained by fitting to EAM data, but, in general, any available experimental or theoretical data could be used. This scheme appears to be well suited to studying equilibrium properties of 2D metallic surfaces via lattice-gas models.

ACKNOWLEDGMENTS

We wish to thank Dr. T. L. Einstein and Dr. H. Zhong for helpful discussions. We also thank T. L. Einstein for bringing Ref. 24 to our attention. This work was supported by U.S. DOE, Office of Basic Energy Sciences, Division of Materials Science, and by the Committee on Research at UC Davis.

*Present address: Physics Dept., Clemson University, Clemson, SC 29634.

[1]P. R. Schwoebel, S. M. Foiles, C. M. Bisson, and G. L. Kellogg, Phys. Rev. B **40**, 10 639 (1989).

[2]A. F. Wright, M. S. Daw, and C. Y. Fong, Phys. Rev. B **42**, 9409 (1990).

[3]G. Grubel, K. G. Huang, D. Gibbs, D. M. Zehner, A. R. Sandy, and S. G. J. Mochrie, Phys. Rev. B **48**, 18 119 (1993).

[4]J. Perdereau, J. P. Biberian, and G. E. Rhead, J. Phys. F **4**, 798 (1974).

[5]T. Michely, M. Hohage, M. Bott, and G. Comsa, Phys. Rev. Lett. **70**, 3943 (1993).

[6]G. Rosenfeld, A. F. Becker, B. Poelsema, L. K. Verheij, and G. Comsa, Phys. Rev. Lett. **69**, 917 (1992).

[7]M. Bott, T. Michely, and G. Comsa, Surf. Sci. **272**, 161 (1992).

[8]R. Kunkel, B. Poelsema, L. K. Verheij, and G. Comsa, Phys. Rev. Lett. **65**, 733 (1990).

[9]M. Villarba and H. Jonsson, Phys. Rev. B **49**, 2208 (1994).

[10]R. Wang and K. A. Fichthorn, Surf. Sci. **301**, 253 (1994).

[11]S. Liu, Z. Zhang, G. Comsa, and H. Metiu, Phys. Rev. Lett. **71**, 2967 (1993).

[12]C.-L. Liu, J. M. Cohen, J. B. Adams, and A. F. Voter, Surf. Sci. **253**, 334 (1991).

[13]The EAM is comprehensively reviewed in M. S. Daw, S. M. Foiles, and M. I. Baskes, Mater. Sci. Rep. **9**, 251 (1993).

[14]R. Fletcher and C. M. Reeves, Comput. J. **7**, 149 (1964).

[15]A. F. Voter, Los Alamos National Laboratory Technical Report No. LA-UR-93-3901, 1993.

[16]A. F. Voter and S. P. Chen, in *Characterization of Defects in Materials,* edited by R. W. Siegel, J. R. Weertman, and R. Sinclair, MRS Symposia Proceedings No. 82 (Materials Research Society, Pittsburgh, 1987), p. 175.

[17]C.-L. Liu and J. B. Adams, Surf. Sci. **268**, 73 (1992).

[18]S. C. Wang and G. Ehrlich, Surf. Sci. **239**, 301 (1992). Wang and Ehrlich observed triangular *and* linear-shaped Ir trimers over a substrate temperature range of 230–255 K, whereas our ($T=0$) Pt calculations strongly favor the triangle over the linear shape by about 0.75 eV (Table I). Triangular Ir hexamers were also observed, whereas we find the triangular hexamer's binding energy to be about 0.05-eV lower than the more elongated ground-state hexamer (Fig. 6). These differences may only be due to differences in the way the two chemically distinct species (Pt and Ir) bond.

[19]On the Pt(001) surface, linear chains are the observed ground-state configurations for Pt clusters with three and five adatoms (Refs. 1 and 2), in contrast to the compact island-shaped clusters found here.

[20]L. Pauling, Phys. Rev. **54**, 899 (1938); A. E. Carlsson and N. W. Ashcroft, Phys. Rev. B **27**, 2010 (1983); G. C. Abell, *ibid.* **31**, 6184 (1985).

[21]For example, the origin of the (1×2) missing-row reconstruction of Au(110) and Pt(110) can be viewed to first order as a competition between attractive second-nearest-neighbor and repulsive three-body nearest-neighbor interactions: S. M. Foiles, Surf. Sci. **191**, L779 (1987); M. S. Daw and S. M. Foiles, J. Vac. Sci. Technol. A **4**, 1412 (1986); also see Ref. 13.

[22]M. W. Finnis and J. E. Sinclair, Philos. Mag. A **50**, 45 (1984).

[23]K. W. Jacobsen, J. K. Norskov, and M. J. Puska, Phys. Rev. B **35**, 7423 (1987).

[24]T. L. Einstein, Langmuir **7**, 2520 (1991), and references therein.

[25]T. B. Grimley, Proc. Phys. Soc. London **90**, 751 (1967); T. L. Einstein, CRC Crit. Rev. Solid State Phys. Mater. Sci. **7**, 261 (1978); J. P. Muscat, Prog. Surf. Sci. **18**, 59 (1985).

[26]W. Y. Ching, D. L. Huber, M. G. Lagally, and G. C. Wang, Surf. Sci. **77**, 550 (1978). Ching *et al.* estimate the magnitude of two trio interactions by assuming they produced the observed asymmetry in the temperature-coverage phase diagram for the O/W(110) system.

[27]In the EAM, this effect has its origin in the positive curvature of the embedding function; see Ref. 13.

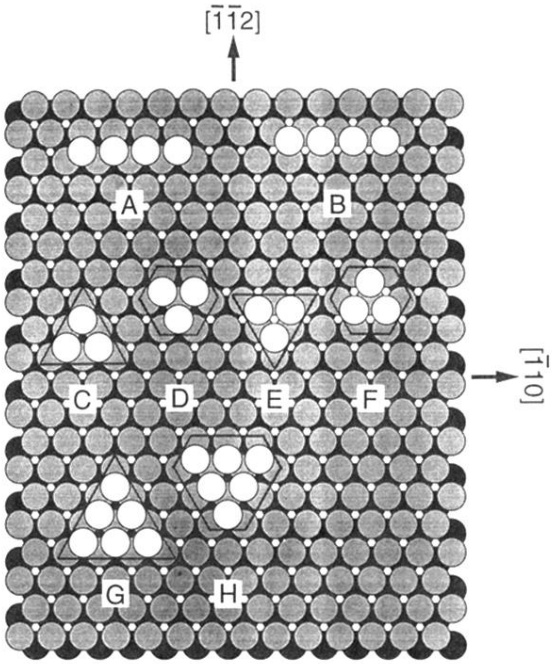

FIG. 1. Several homogeneous-site clusters on the Pt(111) surface as viewed from above along the [111] direction. Pt adatoms (empty circles) are shown lying above the atoms in the first (shaded circles) and second (dark circles) substrate layers (same scheme used in Figs. 2, 3, 6, 8). The four-adatom chain has two configurations, fcc (A) and hcp (B); whereas the trimer and hexamer each have 4: fcc and hcp versions of both "hollow" (C,E,G) and "filled" (D,F,H) configurations (only the fcc examples of the hexamer are pictured).

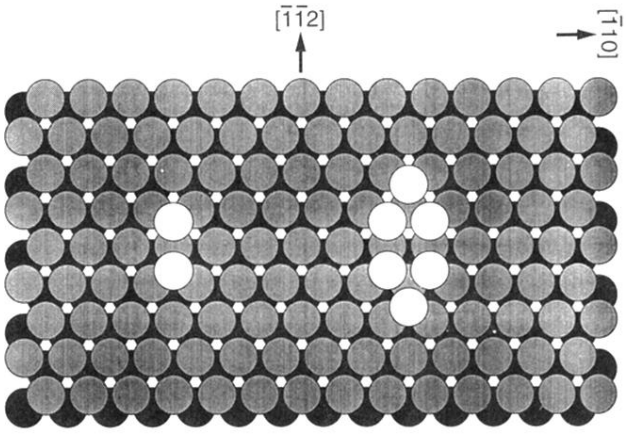

FIG. 2. Two mixed-site clusters on Pt(111) surface; a dimer (left) and hexamer (right).

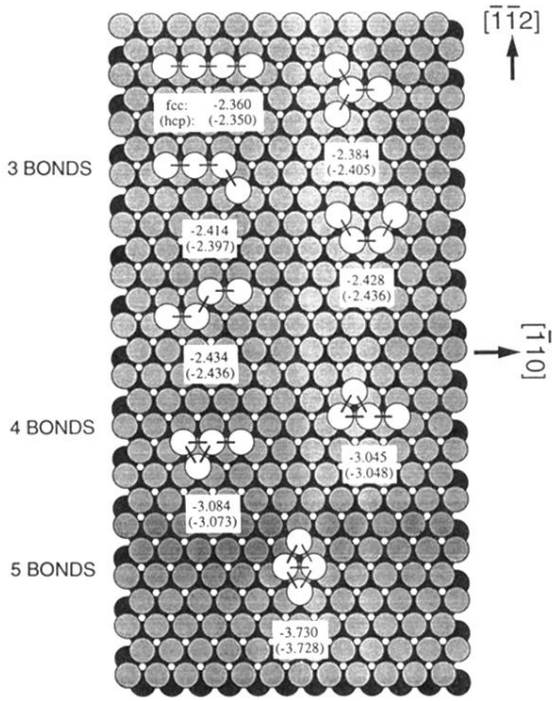

FIG. 3. FCC configurations for *all* the possible (homogeneous-site) four adatom clusters. The binding energies (in eV) for both the fcc and hcp configurations are given below each cluster. The clusters divide into groups (bond families) based on the number of nearest-neighbor bonds (indicated by lines connecting the adatoms) in the cluster. There are five clusters with three bonds, two with four bonds, and one with five.

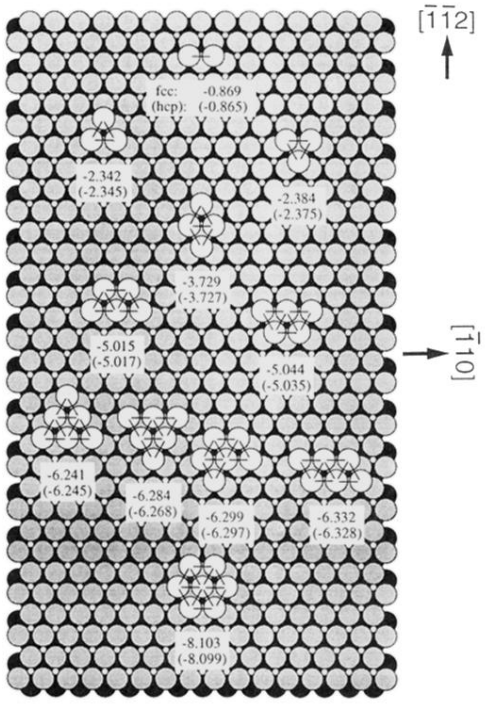

FIG. 6. Predicted fcc ground-state (most stable) cluster configurations and binding energies for both fcc and hcp configurations of Pt clusters with up to seven adatoms. Interadatom bonds are indicated as in Fig. 3..

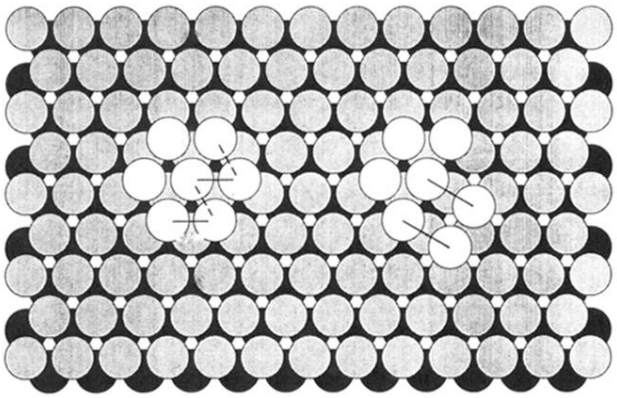

FIG. 8. Diagram illustrating why mixed-site clusters have low binding energies. The energy cost of converting the highly bound hexamer into a mixed-site cluster is about 0.7 eV per shifted adatom for breaking the dashed line bond, and another 0.1 eV for stretching the solid line bond.